Impact of second phase morphology and orientation on the plastic behavior of dual-phase steels

Karim Ismail[a], Astrid Perlade[b], Pascal J. Jacques[a], Thomas Pardoen[a], Laurence Brassart[c,] *

[a] Institute of Mechanics, Materials and Civil Engineering, UCLouvain, 2 Place Sainte Barbe, 1348 Louvain-la-Neuve, Belgium

E-mail: karim.ismail@uclouvain.be, pascal.jacques@uclouvain.be, thomas.pardoen@uclouvain.be

[b] ArcelorMittal Maizières Research SA, Voie Romaine, 57280 Maizières-lès-Metz, France

E-mail: astrid.perlade@arcelormittal.com

[c]Department of Materials Science and Engineering, Monash University, 22 Alliance Lane, Clayton, VIC 3800, Australia

E-mail: laurence.brassart@monash.edu

*Corresponding author.

E-mail address: laurence.brassart@monash.edu (L. Brassart)

ABSTRACT

Martensite volume fraction, composition and grain size are the known primary factors controlling the mechanical behavior of ferrite-martensite dual-phase steels. Recently, excellent performances of dual-phase steels with a fibrous microstructure have been reported. However, the precise role of martensite morphology and orientation has not been thoroughly elucidated yet. This study develops a two-scale micromechanical modeling strategy in order to investigate the effect of particle morphology and orientation on the elastoplastic behavior of dual-phase steels. Finite element simulations are carried out on 3D periodic unit cells, each having a given orientation and volume fraction of spheroidal particles. The overall response is obtained by averaging the response of grains with different orientations, thus bypassing the need for costly full-field simulations on representative volume elements of realistic microstructures. A detailed parameter study systematically investigates the effect of particle morphology and orientation at grain level and at grain assembly level. While particle morphology and orientation effects lead to significant differences at grain level in terms of strain hardening behavior and back-stress development, the impact of the phase morphology at the homogenized multigrain level is almost negligible up to the onset of necking. However, the mechanical fields at the micro-scale are considerably influenced by both particle morphology and orientation, and are expected to largely impact the damage behavior through, among others, generating large grain-to-grain heterogeneities.

Keywords: *dual-phase steels, (A) microstructures, (C) finite elements, (B) elastic-plastic material, (B) inhomogeneous material*

1. INTRODUCTION

Dual-phase steels are heavily used in the automotive industry owing to excellent mechanical properties in terms of strength and ductility, combined with favorable costs resulting from low content in alloying elements and simple processing routes. The good strength-ductility trade-off results from the very different properties of the constituent phases, i.e. ductile ferrite and hard martensite. They confer to dual-phase steels tunable properties involving a moderate to high yield strength depending on martensite content, a high initial hardening rate and no Lüders plateau (Bouaziz et al., 2013; Sakaki et al., 1983).

The mechanical behavior of dual-phase steels is the result of an interplay of mechanisms, dictated by various parameters, including carbon content and distribution in the martensite particles, volume fraction of martensite, ferrite and martensite grain size, and residual stress resulting from processing (Kadkhodapour et al., 2011a; Ramazani et al., 2013). The morphology, shape and orientation of the particles also affect the elastoplastic behavior. The present study focuses on the latter characteristics.

Up to now, experimental investigations mainly focused on the impact of martensite volume fraction, ferrite grain size and carbon content. An increase in martensite volume fraction leads to higher yield and tensile strengths (Chang and Preban, 1985; Davies, 1978; Lai et al., 2016; Mazinani and Poole, 2007; Pierman et al., 2014; Ramos et al., 1979; Sarosiek and Owen, 1984; Speich and Miller, 1979), generally to the detriment of uniform elongation. Grain refinement strengthens the material (Calcagnotto et al., 2010) while carbon content has a more limited influence on the plastic behavior than the latter two parameters (Davies, 1978). An overview on microstructure evolution during processing and on the link with mechanical properties in dual-phase steels can be found in (Tasan et al., 2015).

In contrast, much less research studies have addressed the role of particle morphology on the elastoplastic behavior of dual-phase steels, even though significant effects have been demonstrated. For instance, martensite banding is now known to be detrimental to damage resistance (Bag et al., 1999). On rolled steels, Sun and Pugh (2002) measured a higher strength in the rolling direction and a lower total elongation in the case of a fibrous microstructure of an as-rolled steel, whereas Sarwar and Priestner (1996) observed both an increase in strength and ductility when increasing the aspect ratio of the grains. The increase in strength is confirmed by the work of Zhang et al. (2016) in the case of martensite alignment along the rolling direction. Kim and Thomas (1981) proposed an alternative heat treatment for dual-phase steels leading to an elongated martensite phase arrangement, called the "Thomas fiber" microstructure. Such an arrangement has been shown to have positive effects on the plastic behavior (Das and Chattopadhyay, 2009; Tomita, 1990).

In a recent study, Pierman et al. (2014) systematically investigated the relative contributions of martensite volume fraction, carbon content and second phase morphology in model dual-phase steels. They found that, at high martensite volume fraction (60%), steels with a Thomas fiber microstructure present lower strength but higher ductility than dual-phase steels with equiaxed microstructure at the same volume fraction and martensite carbon content. Pierman (2013) also showed that steels with elongated microstructures exhibit much larger fracture toughness. However, the fundamental origin of the improved mechanical properties of the Thomas fiber microstructure was not elucidated. The general objective of this work is to gain insight into the role of microstructure morphology on mechanical properties of dual-phase steels through computational modeling.

More precisely, this study focuses on microstructures similar to those considered by Pierman (2013) and Pierman et al. (2014). Representative microstructures of model steels with respectively equiaxed and Thomas fiber microstructures are shown in Figure 1, together with the corresponding heat treatment. Martensite particles appear in light grey and ferrite in dark grey. Both microstructures were processed after hot and cold rolling. Equiaxed dual-phase microstructures resulted from a conventional intercritical annealing (Figure 1.a) bringing the recrystallization of the cold rolled microstructure together with the nucleation and growth of the austenite at the ferrite triple junctions and along their grain boundaries. In contrast, Thomas fiber microstructures resulted from a two-stage heat treatment (Figure 1.b) consisting in a full austenitization followed by water quenching. The resulting fully martensitic microstructure was then reheated in the intercritical temperature range where the austenite nucleated and grew along the interfaces between prior martensite laths. A final water quenching then brought the Thomas fibers microstructure with elongated and aligned martensite particles. The Thomas fiber microstructure has been characterized using a serial sectioning procedure, showing that the martensite particles have a platelet shape.

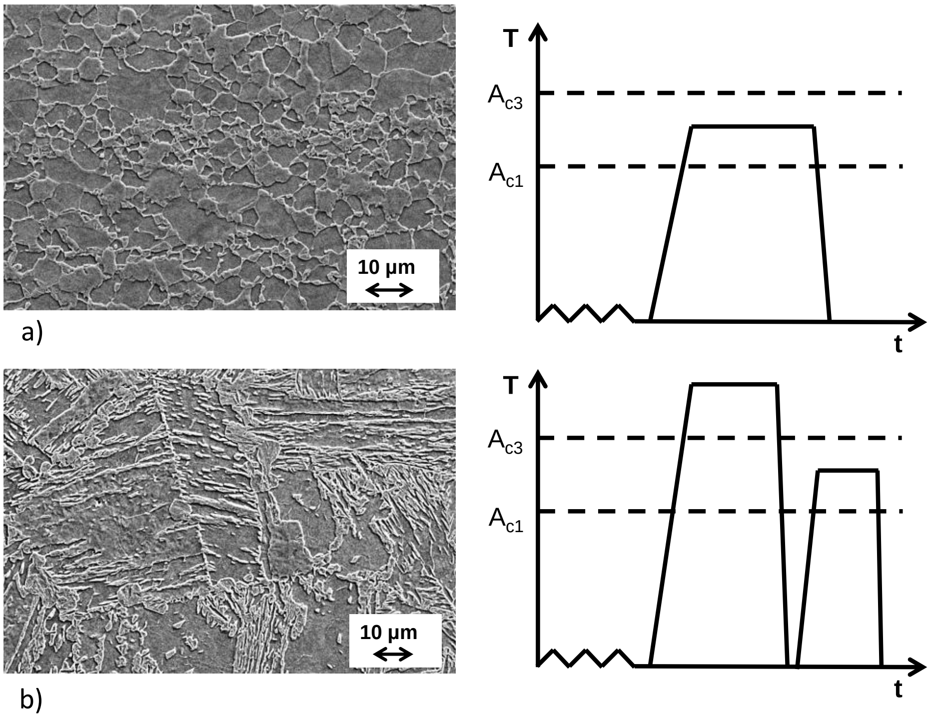

Figure 1. Equiaxed and non-equiaxed microstructures and schematic of the corresponding heat treatments

Semi-analytical homogenization models based on Eshelby's isolated inclusion solution have been repeatedly used to predict the properties of dual-phase steels. For instance, Delincé et al. (2007), Mazinani and Poole (2007) and Pierman et al. (2014) have shown, among other things, that accounting for martensite plastic behavior is essential to accurately predict the overall mechanical response. However, mean field models provide only average mechanical field values. For detailed predictions of the local stress and strain fields, direct Finite Element (FE) analysis on representative microstructures constitutes the most reliable approach. FE calculations can be performed on simple unit cells such as in (Delannay et al., 2006; Lai et al., 2016; Mahnken et al., 2009) assuming a periodic microstructure. FE simulations on random Representative Volume Elements (RVEs) containing many particles can be used to better account for microstructure complexity. Realistic 2D RVEs can be directly built based on SEM micrographs to capture the distribution of martensite as well as morphology variation (Abid et al., 2015; Choi et al., 2009), but generally tend to underestimate the strength. This can be addressed by considering 3D RVEs (Amirmaleki et al., 2016; Bong et al., 2017; Paul and Kumar, 2012) at the expense of larger computational cost. By fully resolving the local stress and strain fields in the microstructure, these simulations can provide detailed insight in the process of plastic localization and damage evolution, see (de Geus et al., 2015; Kadkhodapour et al., 2011b; Sun et al., 2009; Tasan et al., 2014; Zarei et al., 2016). For instance, high stress concentrations near martensite islands can lead to interfacial debonding or fracture of the hard phase; high local stress triaxiality favors void growth; and local imperfections can be the precursors of instability in the form of shear band.

Only few of these computational studies addressed the role of second phase morphology. Ramazani et al. (2012) used FE simulations on 2D RVEs to investigate the effect of martensite bands on the effective properties of dual-phase steels. They found that decreasing the aspect ratio of the bands leads to larger uniform elongation. Pagenkopf et al. (2016) considered equiaxed, elongated and flattened martensite in 3D RVEs loaded in directions parallel and perpendicular to the elongated particles, and concluded that an elongated and a flat martensite morphology lead to a higher strength compared to spherical particles. Abid et al. (2017) considered 2D RVEs with equiaxed and elongated martensite particles, predicting an increase of strength and ductility with the elongated morphology.

The main disadvantage of full-field simulations on realistic microstructures is the large computational cost, especially for 3D simulations. Also, such simulations, in general, do not allow a systematic investigation of the effect of single parameters (such as individual particle orientation) as these are coupled to one another, depending on the location of the particle in the RVE. As an alternative, an original two-step approach has been recently proposed by Ognedal et al. (2014) in the context of a study of void nucleation and growth in mineral filled PVC. In this approach, simplified unit cells were assembled to represent a staggered array of spherical particles, reducing the computational cost compared to an RVE. This approach has been recently extended by Hatami et al. (2017) for application to multiphase TRIP steels. A similar approach is adopted in the present study to model dual-phase steels with elongated and flat martensite.

The objective of the paper is to present a systematic investigation of the effect of particle shape and orientation on both the effective plastic behavior and the local mechanical fields of dual-phase steels. We developed a two-level homogenization approach involving FE calculations on unit cells, in the spirit of the approach of Ognedal et al. (2014). The first level is the one of a pseudo-grain in which the martensite particles are all oriented in the same direction, see Figure 1.b. The second level is the macroscopic level, consisting of a collection of grains with different particle orientations. The focus is on the impact of particle shape and orientation on the flow stress, uniform elongation, strength-ductility product and back-stress. Local fields within pseudo-grain are investigated in terms of local stress triaxiality, maximum principal stress and plastic strain distribution, which control damage evolution. Although the focus is on dual-phase steels, some of the results are of interest for other classes of metallic alloys such as various α/β Ti alloys or metal matrix composites with short fibers.

The paper is organized as follows. The modeling approach and averaging procedure are described in Section 2. Results of the parametric study are given in Section 3, at both grain level (where all particles have the same orientation) and at macroscopic level (where grains with particles of different orientations are considered). The model and its results are discussed in Section 4, before concluding.

2. MODEL DESCRIPTION

2.1. Two-level modeling approach

The modeling strategy is schematically represented in Figure 2. The microstructure of interest is made of martensitic particles with a platelet shape. In such microstructures resulting from the two-stage heat treatment explained in the introduction, the martensite particles developing inside the same parent austenitic grain exhibit the same shape and orientation. Therefore, the microstructure is virtually decomposed into a set of "grains" made of matrix and of one specific particle shape and orientation relative to a macroscopic coordinate system.

The two-level computational strategy is based on the generation of a wide range of unit cells, each one representing a grain, in which the microstructure is assumed periodic, consisting of a regular array of spheroids (Figure 2). Within each cell, three parameters are independently varied, namely the particle aspect ratio (*ar*), orientation (θ) and martensite volume fraction ($V_{\alpha'}$). Each unit cell is subject to uniaxial tension in the direction 1 of the macroscopic reference system. The effective response of the aggregate of grains is obtained by averaging the stress over all unit cells. In the averaging procedure, a weight is attributed to the response of each cell depending on its importance in the distribution of orientations. This method has the advantage of being fully 3D without being too computationally intensive. More details about the definition of the parameters, the FE procedures and the averaging procedure are given in Section 2.2.

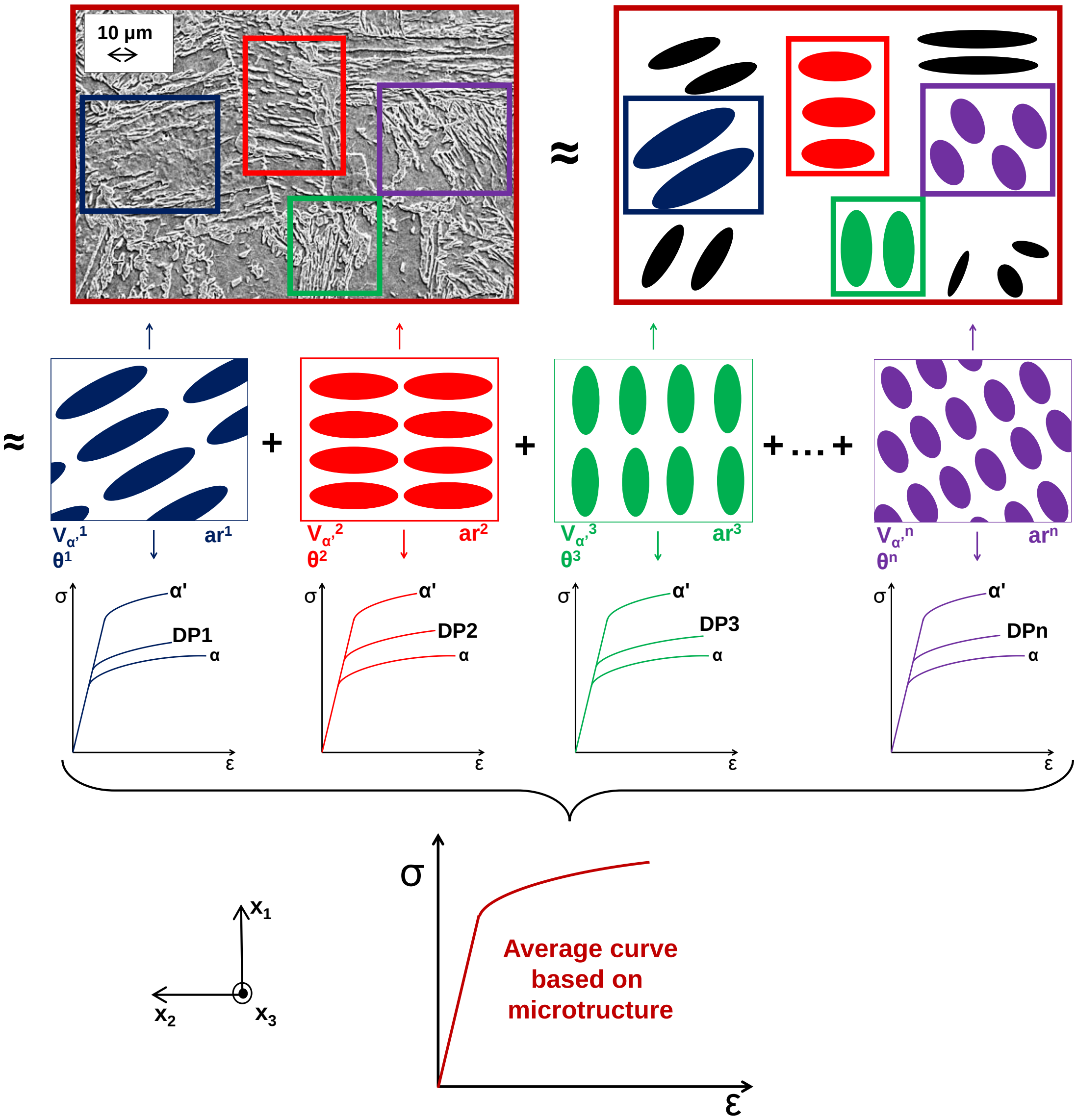

Figure 2. Schematic of the proposed two-level computational strategy for a generic dual-phase microstructure. The microstructure is represented by a set of *n* pseudo-grains with martensite volume fraction $V_{\alpha'}^{i}$ (*i=1,...n*). The microstructure of each grain is taken as a regular arrangement of identical spheroidal particles having all the same aspect ratio ar^i and orientation θ relative to the macroscopic loading direction.

2.2. Unit cell description

Thanks to the periodicity of the microstructure within each pseudo-grain, each unit cell consists of a parallelepiped box containing a single spheroidal particle surrounded by matrix material. Thus, the main directions of the particle are aligned with the edges of the cell. Note that this is different from the schematic representation in Figure 2, in which the particle orientation within each cell varies from cell to cell. In view of FE calculations using periodic boundary conditions, it is much more convenient to always consider particles to be aligned with the cell edges, and, instead, vary the loading direction relative to the spheroid axes. The unit cell is described by three parameters:

- **Aspect ratio "*ar*".** The aspect ratio of the spheroidal particle is defined as the ratio of the long axis to the short axis in the case of a prolate spheroid ($ar > 1$), and as the ratio of the short axis to the long axis in the case of an oblate spheroid ($ar < 1$). The unit cell is given the same aspect ratio as the particle. In other words, the effect of the relative particle spacing between particles at constant aspect ratio is not investigated. Note also that the considered particle stackings are not isotropic, even in the case of spherical particles, which are aligned in a cubic array. The ratio of the cell edges can then be deduced from the volume fraction and aspect ratio of the particle (the actual size of the cell is not relevant since the constitutive models used in this work do not include any internal length. Four aspect ratios have been selected: i) $ar = 1$ (spherical particles); ii) $ar = 0.2$ (platelet-like particles); iii) $ar = 2$ and $ar = 6$ (fiber-like particles).
- **Orientation angle "θ".** Uniaxial loading of the unit cell is performed at varying angles relative to the spheroid axes in order to determine the effect of particle orientation. As shown in Figure 3, θ is defined as the angle between the macroscopic loading direction and the direction of the particle revolution axis. In the case of an oblate spheroid, the revolution axis is the short axis while it is the long axis for a prolate spheroid. Angles equal to 0°, 30°, 45°, 60° and 90° have been considered.

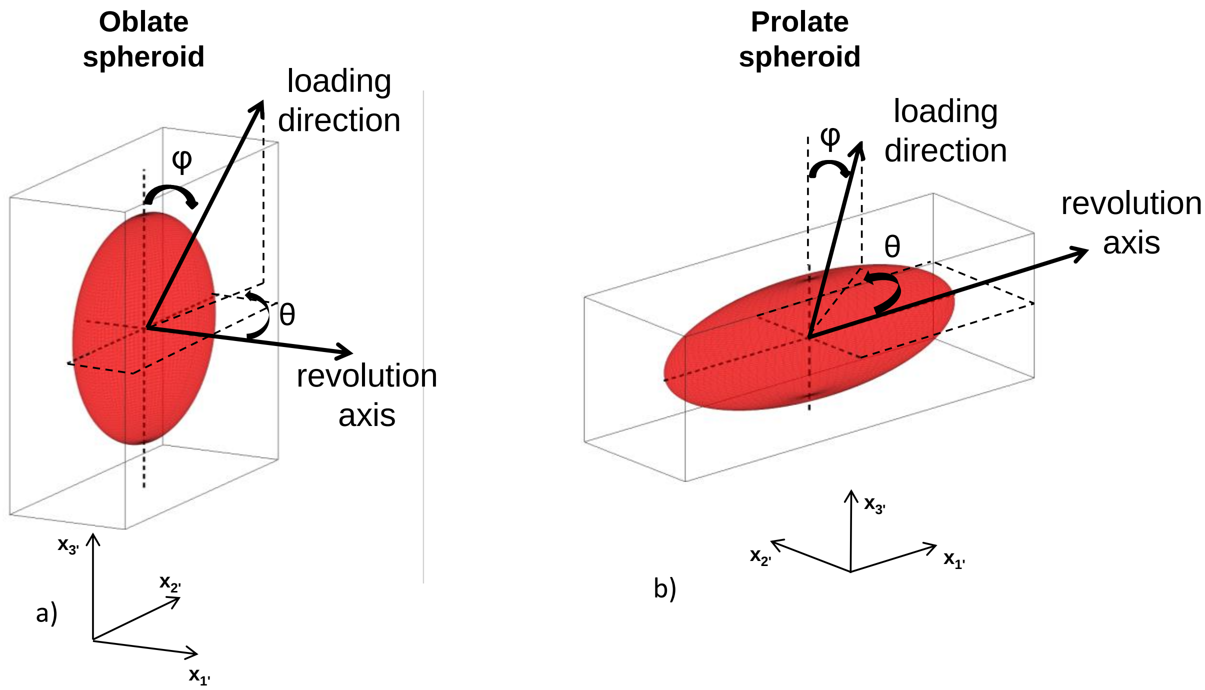

Figure 3. Definition of loading direction θ relative to the revolution axis of the spheroid in the case of a) an oblate spheroidal particle, b) a prolate spheroidal particle

- **Martensite volume fraction "$V_{\alpha'}$".** $V_{\alpha'}$ is varied by changing the size of the particle at constant cell size. For low to moderate volume fraction of martensite (up to 50%), we assumed a martensite particle within a ferrite matrix. The role of martensite as a particle phase becomes however questionable at larger volume fractions, where martensite connectivity arises. In order to take this percolation effect into account, the roles of matrix and particles are reversed in the numerical simulation at martensite volume fractions larger than 50%, with the martensite being treated as the matrix and the ferrite as the particle. The considered values for the martensite volume fraction are $V_{\alpha'}$ = 10%, 20%, 30%, 45% (martensite particle) and 55% and 70% (ferrite particle).

The effective response of the kth unit cell (*k=1,...,n*) is calculated using the FE method. Periodic boundary conditions are imposed and expressed as

$$u_{i'}^{+} - u_{i'}^{-} = \varepsilon_{i'j'}^{(k)} \left(x_{j'}^{+} - x_{j'}^{-} \right) \tag{1}$$

where $\boldsymbol{u}$ is the displacement vector on the cell boundary, $\boldsymbol{x}$ refers to the position of the nodes on the boundary and superscripts + and - indicate corresponding points on either side of the unit cell. According to a classical result in homogenization theory, the strain tensor $\boldsymbol{\varepsilon}^{(k)}$ then coincides with the volume average of the microscopic strain field within the unit cell. In Eq. (1), the primed indices denote components in a *local* coordinate system with axes aligned with the edges of the unit cell. The effective stress applied to the unit cell, $\boldsymbol{\sigma}^{(k)}$ is then calculated as the volume average of the local stress field within the unit cell.

The unit cell is subject to uniaxial tension in the macroscopic direction 1, which makes an angle θ with the particle revolution axis. In a strain-driven approach, this means that only the component $\varepsilon_{11}^{(k)}$ is known a priori (unprimed indices indicate components in the macroscopic coordinate system). The other components of strain $\varepsilon_{ij}^{(k)}$ are determined iteratively in such a way that the stress state $\sigma_{ij}^{(k)}$ is uniaxial, with $\sigma_{11}^{(k)}$ the only non-zero component. All unit cells are thus subject to the same macroscopic strain $\varepsilon_{11}^{(k)} = \varepsilon_{11}$, whereas the other components $\varepsilon_{ij}^{(k)}$, as well as the stress $\sigma_{11}^{(k)}$, differ from cell to cell. Components of strain (stress) in the macroscopic and local coordinate systems are related by the usual transformation rules for second-order tensors.

Periodic FE meshes with second-order tetrahedra elements were generated using the software Netgen (Schöberl, 1997) and the FE simulations were carried out using the FE software Abaqus (ABAQUS) using C3D10M elements. The periodic condition (1) and the transformation rules between local and macroscopic coordinate systems were implemented through the use of the keyword EQUATION in ABAQUS, together with fictitious nodes undergoing a displacement representing the a priori unknown components of macroscopic strain. The number of elements in the meshes for a spherical particle, prolate particle and oblate particle were approximately 7500, 67000 and 62000, respectively. Unit cell calculations have been performed for every combination of the parameters mentioned above. This database can certainly be extended in future works to other parameters.

2.3. Phase behavior

The elastic response of ferrite and martensite is assumed linear and isotropic with Young's modulus E = 200 GPa and Poisson's ratio ν = 0.3, identical for both phases. Classical J_2 flow theory is used to describe the plastic flow behavior of both ferrite and martensite.

The hardening behavior of martensite is described by an exponential law:

$$\sigma_{y,\alpha'} = \sigma_{y0,\alpha'} + k_{\alpha'}(1 - \exp(-p\, n_{\alpha'})) \tag{2}$$

where $\sigma_{y,\alpha'}$ is the current yield strength, p the accumulated plastic strain, and $n_{\alpha'}$ the hardening exponent. The initial yield strength $\sigma_{y0,\alpha'}$ and hardening parameter $k_{\alpha'}$ (in MPa) depend on the martensite carbon content $C_{\alpha'}$ (in wt%) according to

$$\sigma_{y0,\alpha'} = 300 + 1000 C_{\alpha'}^{1/3} \tag{3}$$

and

$$k_{\alpha'} = (1/n_{\alpha'})\left[a + \frac{bC_{\alpha'}}{1 + (C_{\alpha'}/C_0)^q}\right] \tag{4}$$

where a = 33.10^3 MPa, b = 36.10^4 MPa, C_0 = 0.7, q = 1.45 and $n_{\alpha'}$ = 120. The hardening model (2)-(4) and parameter values are borrowed from Pierman et al. (2014). Best-fit parameters were obtained based on experimental tensile testing data for fully martensitic bulk samples with varying carbon contents. A comparison with experimental curves can be found in that paper. All results shown in the following were obtained for a martensite carbon content $C_{\alpha'}$ equal to 0.15wt%.

The hardening law of ferrite is expressed by Voce's law supplemented by a stage-IV hardening regime:

$$\sigma_{y,\alpha} = \sigma_{y0,\alpha} + (\theta_\alpha/\beta)\big(1 - exp(-\beta\, p)\big) \quad \text{for} \quad \sigma_{y,\alpha} \le \sigma_y^{tr}, \tag{5}$$

$$\sigma_{y,\alpha} = \sigma_y^{tr} + \theta_{IV}(p - \varepsilon^{tr}) \qquad \text{for} \quad \sigma_{y,\alpha} \ge \sigma_y^{tr} \tag{6}$$

where σ_y^{tr} and ε^{tr} are respectively the flow stress and the plastic strain at the transition between stage-III and stage-IV hardening and are given by

$$\sigma_y^{tr} = \sigma_{y0,\alpha} + \frac{\theta_\alpha - \theta_{IV}}{\beta}, \tag{7}$$

$$\varepsilon^{tr} = \frac{1}{\beta} ln(\theta_\alpha/\theta_{IV}), \tag{8}$$

and where $\sigma_{y0,\alpha}$ is the initial yield strength of ferrite, θ_α is the initial work-hardening rate, β is the dynamic recovery coefficient and θ_{IV} is the hardening rate during stage-IV. The values used for the ferrite parameters, identified by fitting the experimental data, were taken from (Lai et al., 2015): $\sigma_{y0,\alpha} = 250$MPa ; $\theta_\alpha = 4900$MPa ; $\beta = 11$; $\theta_{IV} = 100$MPa.

2.4. Effective properties

2.4.1. Averaging over particle orientations distribution

The effective response of the steel is obtained by averaging the stress in the direction of macroscopic loading predicted by a series of unit cells corresponding to various particle orientations. In this study, we assumed that the martensite volume fraction and particle aspect ratio is the same in all the unit cells.

We define σ_{mean} as the macroscopic stress in the direction of loading, averaged over all particle orientations. For a uniform isotropic distribution of particle orientation, averaging of the macroscopic stress component σ_{11} inside each grain over each particle orientation expresses as:

$$\sigma_{mean} = (1/4\pi)\int_0^{2\pi}\int_0^{\pi}\sigma_{11}(\varphi,\theta)sin\theta d\theta d\varphi, \tag{9}$$

where $\sigma_{11}(\varphi,\theta)$ represents the average stress in a unit cell in which the macroscopic loading direction relative to the spheroid principal axes is described by the two angles (φ,θ) , see Figure 3. The periodicity of the unit cell implies that the particles are arranged in a rectangular packing. Therefore, the effective response of a unit cell is not exactly transversely isotropic, since the distance between the particles differs with the angle φ. However, to limit the computational cost, we only considered the case φ=0° and assumed transverse isotropy, i.e.:

$$\sigma_{mean} \approx \frac{1}{2}\int_0^{\pi}\sigma_{11}(\theta)sin\theta d\theta. \tag{10}$$

In practice, simulations have been carried out for a limited number of angles only (see Section 2.2.). A weight was attributed to each orientation in order to represent a uniform distribution of angles. The integral in Equation (10) is approximated as:

$$\sigma_{mean} = (1/2).2\left[\int_{0°}^{15°}\sigma_{11}(0°)\sin(\theta)d\theta + \int_{15°}^{37.5°}\sigma_{11}(30°)\sin(\theta)\,d\theta + \int_{37.5°}^{52.5°}\sigma_{11}(45°)\sin(\theta)\,d\theta \right.$$
$$\left. + \int_{52.5°}^{75°}\sigma_{11}(60°)\sin(\theta)\,d\theta + \int_{75°}^{90°}\sigma_{11}(90°)\sin(\theta)d\theta\right]. \tag{11}$$

2.4.2. Determination of the mechanical properties

Mechanical properties are calculated at both grain level and aggregate level. Investigating mechanical properties at the level of a single unit cell is interesting for two reasons: i) to help understanding the trends for the aggregate response; ii) to gain insight into the limit case of a dual-phase steel with strong morphological anisotropy.

a. Flow stress at different levels of plastic deformation and at the onset of necking. All values are given in terms of true stress and true (logarithmic) strain. The yield strength $\sigma_{0.2}$ is taken as the stress at 0.2% of plastic strain. Likewise, the flow stresses σ_1 and σ_5 are defined at 1% and 5% of plastic strain. The tensile strength σ_u and the associated uniform elongation ε_u are estimated using the Considère criterion

$$\frac{d\sigma}{d\varepsilon} = \sigma. \tag{12}$$

b. Back-stress. The contrasted phase properties lead to the development of heterogeneous plastic strains and hence back stresses. Back stresses are responsible for the Bauschinger effect, which consists in a reduction of the effective flow stress during reverse loading. Reverse loading simulations were systematically conducted following a 10% pre-straining, and the following measure of back-stress was used (Moan and Embury, 1979):

$$\sigma_b = \frac{\sigma_{ref} - |\sigma_{be}|}{2}, \tag{13}$$

in which σ_{be} is the reloading yield strength at 0.2%, called the back extrapolated stress, and σ_{ref} is the maximum value of stress reached in monotonic loading prior to unloading, called the reference stress, see Figure 4. Back-stresses contribute to the strain hardening capability.

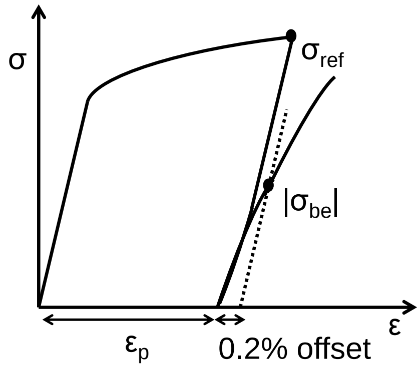

Figure 4. Definition of the parameters used to define the magnitude of the back-stress

2.5. Extraction of local fields

The analysis focuses on three local field quantities, namely the accumulated plastic strain p, the maximum principal stress σ_I and the stress triaxiality T. The latter is defined as

$$T = \sigma_h/\sigma_{eq} \tag{14}$$

where σ_h is the hydrostatic stress and σ_{eq} is the von Mises equivalent stress. These three parameters are known to be the primary elements controlling the process of damage. A damage indicator D, motivated by the Rice and Tracey void growth law (Rice and Tracey, 1969), is calculated as

$$D = \int_0^p exp((3/2)\,T)dp'. \tag{15}$$

The magnitude of these parameters can be evaluated at all points in the cell, but we will in particular look at the pole of the particle on the revolution axis where they can attain especially high values due to stress and strain concentration. It is to be noted that the Lode angle parameter, which is not investigated here, can also largely influences damage behavior (Bai and Wierzbicki, 2008; Erice and Gálvez, 2014; Pineau et al., 2016; Xue, 2007).

3. PARAMETER STUDY

3.1. Effect of particle orientation on mechanical properties at grain level

3.1.1. Stress-strain response

The predicted stress-strain curves of unit cells corresponding to different loading orientations are given in Figure 5 up to the onset of necking together with the variation of the hardening rate as a function of strain. Figure 5.a shows that for spherical martensite particles, the hardening capacity decreases when increasing the angle θ from 0° to 45°. Once the threshold value of 45° is reached, increasing further θ up to 90° leads to the opposite trend. The difference between the responses comes from the non-isotropic distribution of particles as explained in Section 2.2.

Figures 5.b and c, for the case of prolate and oblate particles respectively, show that the same trend applies to non-spherical particles, i.e. that the 0° and 90° orientations lead to a larger strain hardening capacity than the 30° and 60° responses which in turn have a larger strain hardening capacity than the 45° response. Besides, the behaviors for θ equal to 0° and 90° (or 30° and 60°) do not coincide as in the case of spherical particles, due to a reduced symmetry of the cells when the particle shape is not spherical. The importance of the difference between these responses varies with aspect ratio and martensite volume fraction.

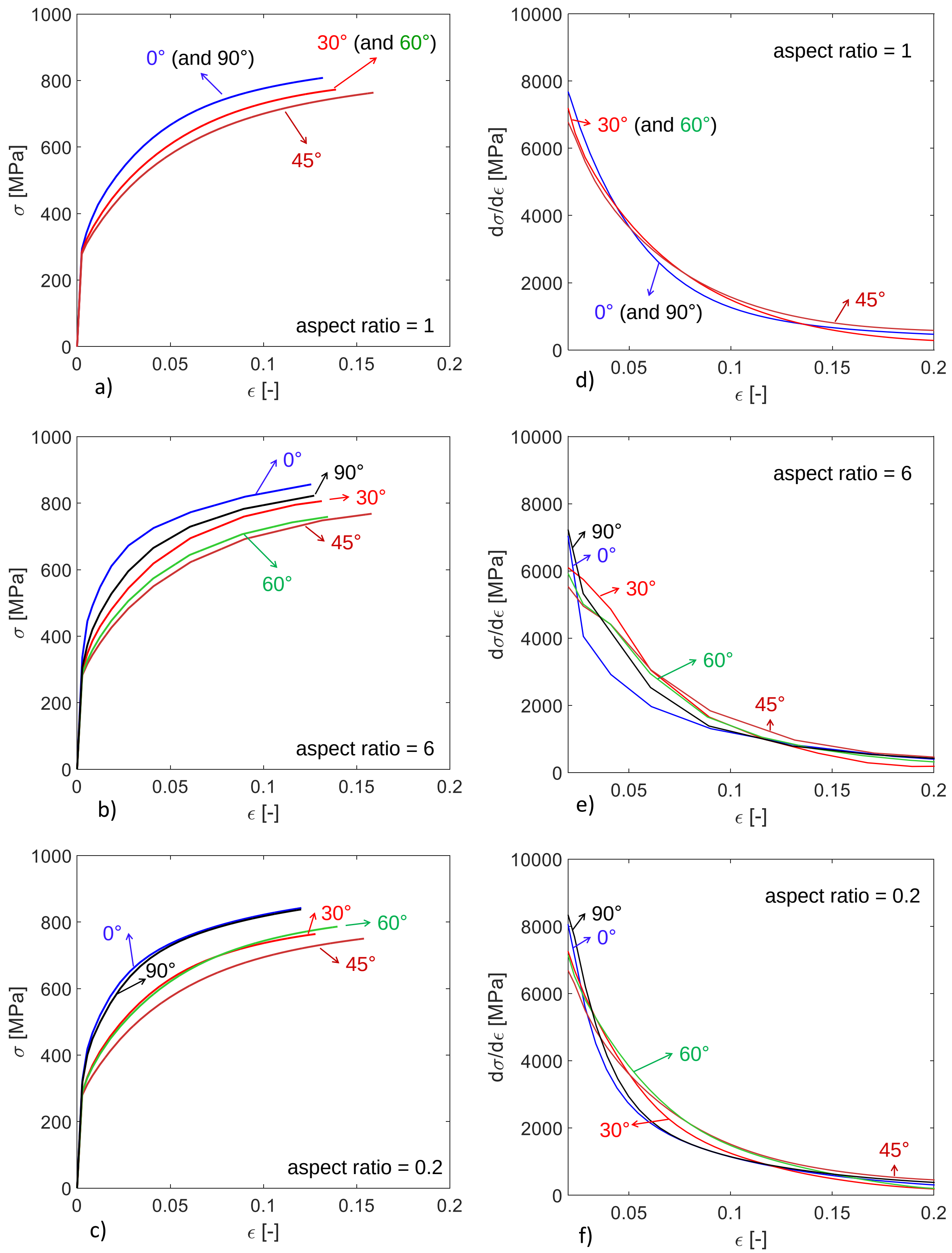

Figure 5. Stress-strain response and derivative of stress with respect to strain for various loading directions θ in the case of elementary cells with $V_{\alpha'}$ = 30% and involving: a) and d) spherical martensite particle, b) and e) prolate martensite particle, c) and f) oblate martensite particle

3.1.2. Strength and ductility

Figure 6 shows the variations of the yield strength $\sigma_{0.2}$, the tensile strength σ_u, as well as σ_1 and σ_5 reference strength levels, and ε_u as a function of θ. Figures 6.a and b are for a ferritic matrix ($V_{\alpha'}$ = 30%) and Figures 6.c and d for a martensitic matrix ($V_{\alpha'}$ = 70%). In agreement with the results of Figure 5, the hardening capacity decreases from 0° to 45° and increases again up to 90°. Ductility is the highest at 45° and the strength is the lowest. Furthermore, spherical particles almost always exhibit the lowest strength and the highest ductility for a ferrite matrix. The higher strength in the 0° and 90° orientations compared to ~45° is due to a higher hardening rate around 0° and 90° orientations at small strains, and the higher ductility around 45° is due to a higher hardening rate in the ~45° orientation at higher strains, see Figures 5.d to f. Departing from an aspect ratio of 1 increases the strength and decreases the ductility. The effect of the aspect ratio is opposite when martensite plays the role of matrix. But, in both cases, the effect of orientation increases when departing from an aspect ratio of 1. These results show that orientation effects can lead to grain to grain strength differences, sometimes up to more than 20%. And, in the case of a martensitic matrix, the ductility ε_u almost doubles between 0° and 45° for very prolate or very oblate ferrite particles.

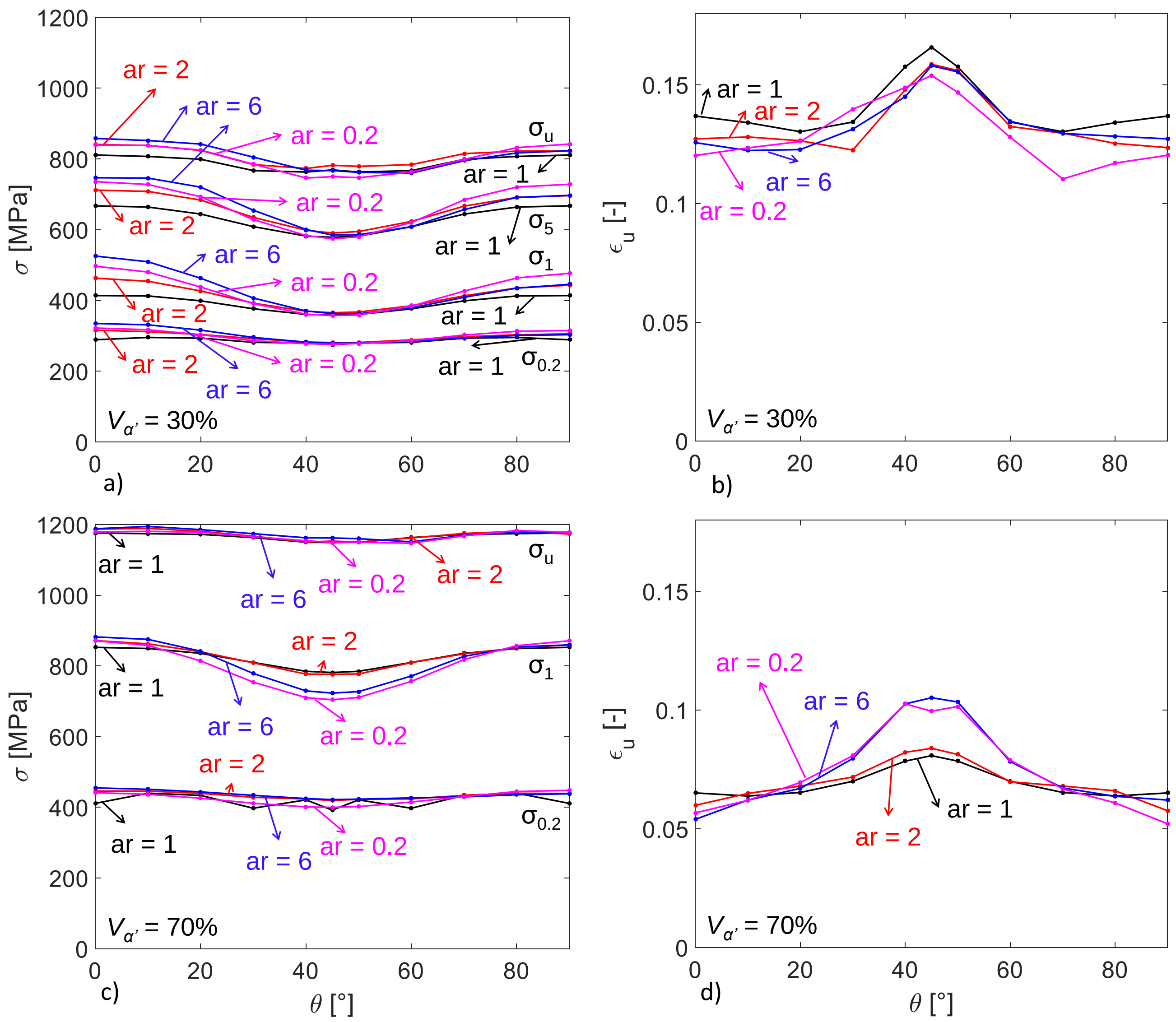

Figure 6. Summary of the main flow properties for elementary unit cells as a function of loading direction θ. a) Yield strength at various strains for a ferritic matrix, b) uniform deformation for a ferritic matrix, c) yield strength at various strains for a martensitic matrix, d) uniform deformation for a martensitic matrix

3.1.3. Magnitude of the back-stress

Figure 7 shows the back-stress σ_b generated by a pre-strain of 0.1 as a function of the orientation for three particle aspect ratios. In the case of a ferritic matrix (Figure 7.a), the magnitude of the back-stress is significantly amplified in non-equiaxed particles, especially near the 0° and 90° orientations. This means that internal stresses are larger for oblate and prolate particles, because the absence of sharp particle tips in equiaxed microstructures and a lower confinement of the ferrite matrix in the vicinity of the tips leads to more homogeneous stress distribution. The larger kinematic hardening contribution (i.e. large back-stresses) probably explains the larger strain hardening capacity at small strains. In the case of a martensitic matrix (Figure 7.b), the magnitude of the back-stress is larger for equiaxed particles for most orientations, explaining the higher strain hardening capacity at small strains in the equiaxed microstructure steels. Here again, the variation of back-stress with orientation is more significant for non-equiaxed particles. However, the order of magnitude of the back-stress is about the same for both a ferritic and martensitic matrix. But, compared to the yield stress, its amplitude is much lower in the case of a martensitic matrix. A smaller back-stress is expected for a hard matrix embedding softer particles. The reason is that the hard matrix then contributes more to deformation, thereby decreasing the plastic deformation mismatch, and thus the ensuing back-stress.

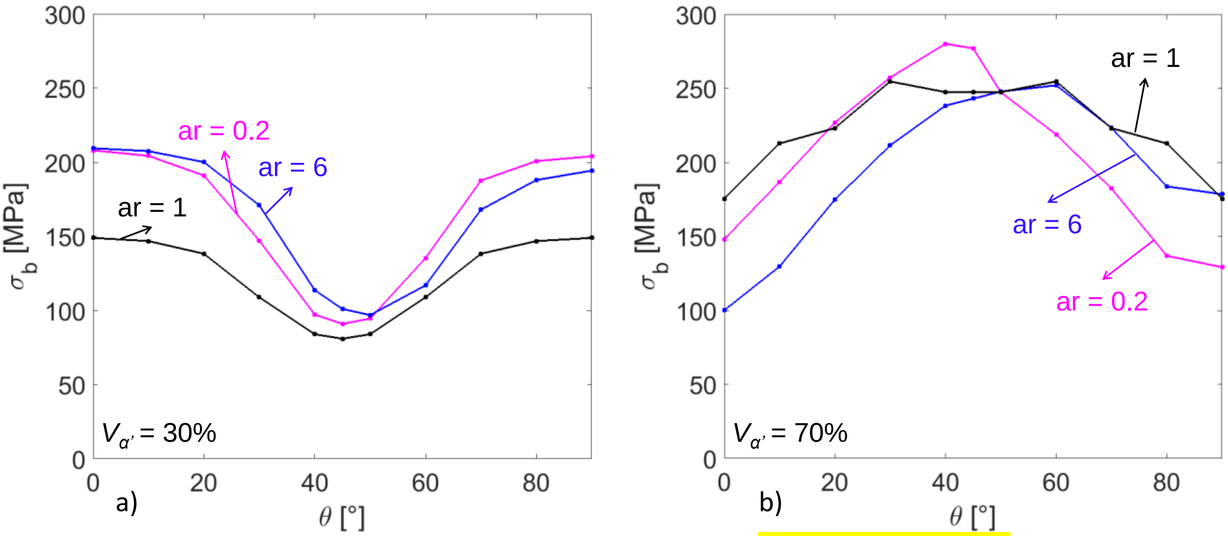

Figure 7. Effect of the loading orientation and particle aspect ratio on the magnitude of the back-stress for a) a ferritic matrix, b) a martensitic matrix

In addition to Figure 7, Figure 8 shows that there is less (resp. more) back-stress at 45° than at 0° when the particle phase is made of hard martensite (resp. the softer ferrite). The effect on the macroscopic curve is more pronounced in the case of a ferritic matrix ($V_{\alpha'}$ = 30%). This is because back-stress essentially builds up in the softer ferrite, which contribution is low in the case of the martensitic matrix ($V_{\alpha'}$ = 70%).

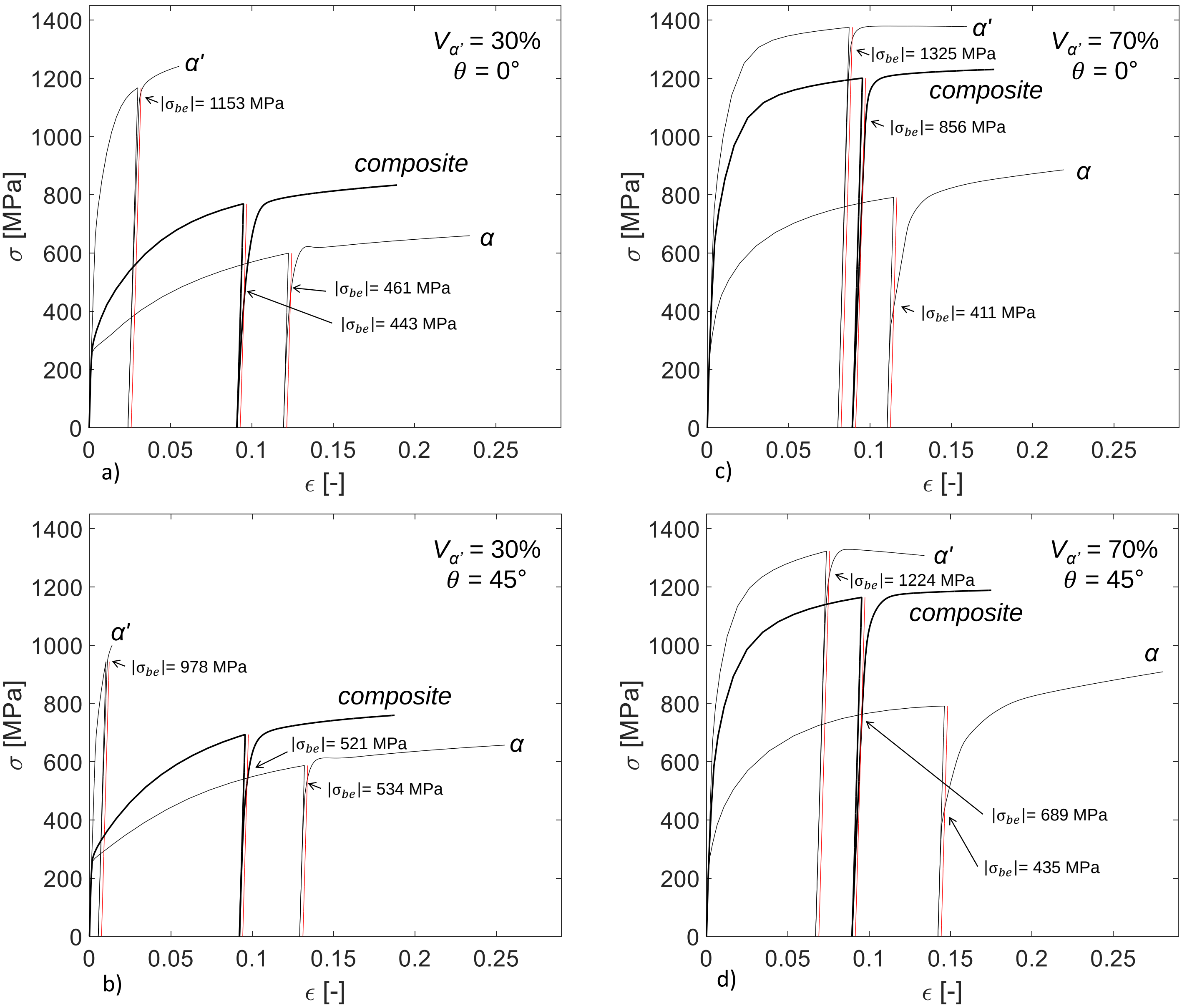

Figure 8. Back-stress level at an overall prestrain of 0.1 in the ferrite phase, martensite phase and full unit cell for a) 30% $V_{\alpha'}$ and a 0° θ, b) 30% $V_{\alpha'}$ and a 45° θ, c) 70% $V_{\alpha'}$ and a 0° θ, d) 70% $V_{\alpha'}$ and a 45° θ

3.2. Impact of martensite volume fraction and aspect ratio on aggregate response

The response of, on the one hand, an aggregate of several grains with different martensite lath orientations in a ferritic matrix ($V_{\alpha'}$ = 30%), and, on the other hand, of ferrite particles embedded inside a martensitic matrix ($V_{\alpha'}$ = 70%), are addressed in Figure 9 for different aspect ratios. Figures 9.a and b show the stress-strain response for the ferritic and martensitic matrix, respectively. Figures 9.c and d show the magnitude of the flow stress at different strains for the ferritic and martensitic matrix, respectively. Figures 9.e and f show the effect of particle aspect ratio on the ductility and on the $\sigma_u \varepsilon_u$ product, respectively. The morphology of the second phase has some effects on the aggregate behavior:

- The strain hardening capacity of the dual-phase steels increases at small deformation when the martensite particle aspect ratio differs from 1. A decrease of the strain hardening capacity at small deformation with increasing particle aspect ratio is observed in the case of a martensitic matrix. For a martensitic matrix, the reversed trend is observed due to the fact that martensite then accommodates a larger part of the deformation. Indeed, the ferrite becomes more spatially confined when the aspect ratio differs from unity, especially around the regions of high curvature at the spheroid tips. Hence, the ferrite phase is forced to follow the deformation of the martensite matrix and the deformation mismatch thus decreases.
- Figures 9.c to f show that very prolate particles lead to a behavior similar to very oblate particles, hence particle morphology acts roughly through the ratio between the length of the longest to the shortest axis.
- Figure 9.e shows that the uniform elongation varies opposite to the strength regarding the effect of aspect ratio. This leads to a relatively constant product $\sigma_u \varepsilon_u$ in the case of a ferritic matrix as seen in Figure 9.f. In the case of a martensitic matrix however, an increase of the $\sigma_u \varepsilon_u$ product by about 10% is found when departing from the spherical shape. This is due to the larger variation of

uniform elongation with orientation for very prolate or very oblate particles, which doubles between 0° and 45°, see Figure 6.d).

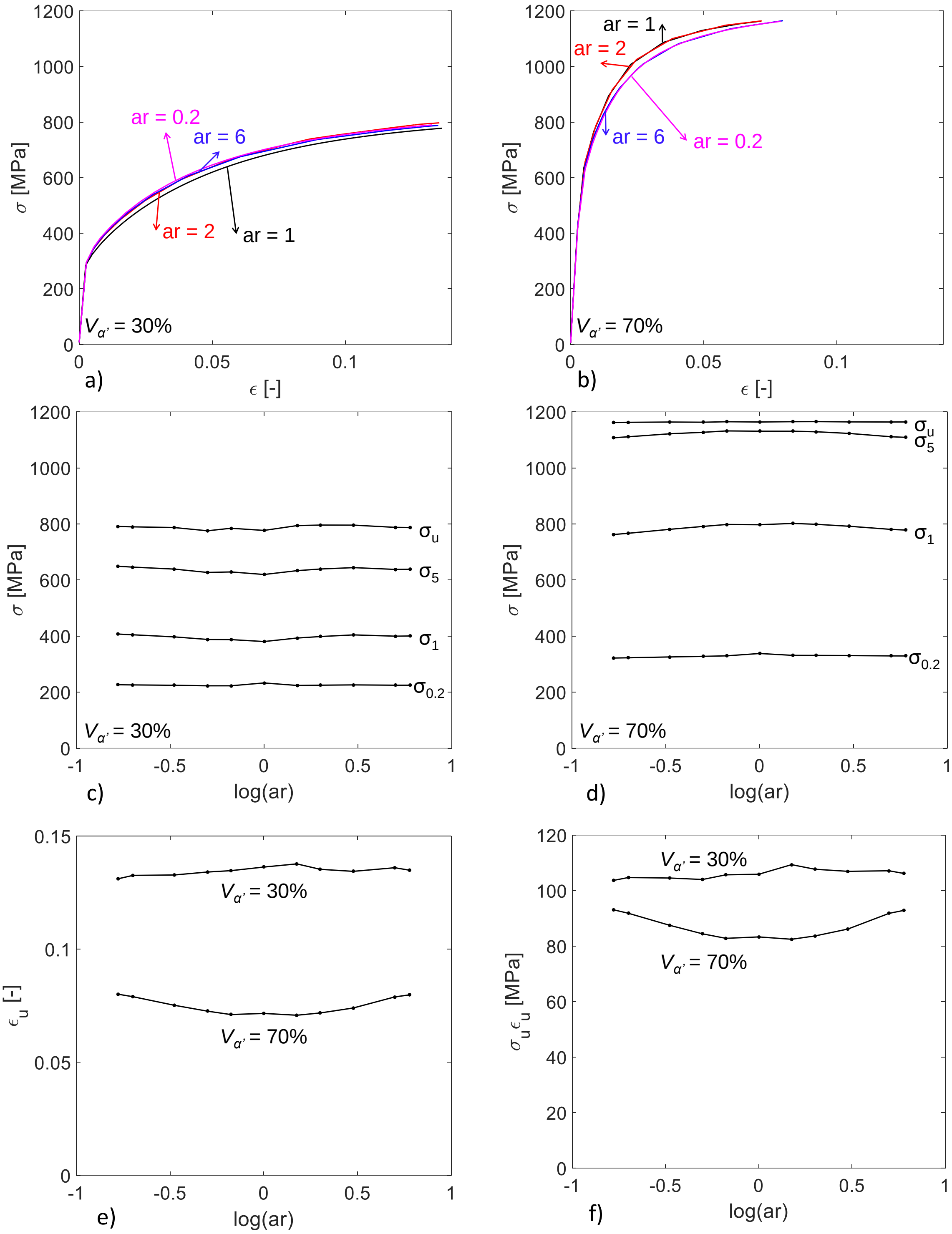

Figure 9. Effect of the particle aspect ratio on the response of dual-phase steels with a uniform distribution of particle orientations in terms of a) uniaxial stress-strain behavior for a ferritic matrix, b) uniaxial stress-strain behavior for a martensitic matrix, c) flow stress at different strains for a ferritic matrix, d) flow stress at different strains for a martensitic matrix, e) uniform deformation, f) product $\sigma_u \varepsilon_u$

The most important conclusion at this stage of the analysis is that the impact of martensite morphology on the aggregate hardening behavior is small (see discussion) when the distribution of second phase arrangement and spatial arrangement is isotropic while much larger effects are found at the “grain” level with aligned particles. All these results were obtained for a martensite carbon content equal to 0.15wt%. Calculations have been repeated for a martensite carbon content equal to 0.6wt%, showing a slightly larger but still limited effect.

3.3. Local fields analysis

Figure 10 shows contour plots of the local accumulated plastic strain p and of the maximum principal stress σ_I in deformed unit cells for several aspect ratios and identical martensite volume fraction and orientation ($V_{\alpha'}$ = 30% ; θ = 0°). The contour plots correspond to a macroscopic strain of 0.1. One eighth of a particle is present at every corner of the cell. Extreme differences in the local values can be found within one unit cell. The ferrite-martensite interface is systematically undergoing the largest plastic strains on the soft ferrite side, and, in the particular case of a spherical martensite particle at 0°, the center of the ferrite ligament in the direction of loading also undergoes large strains.

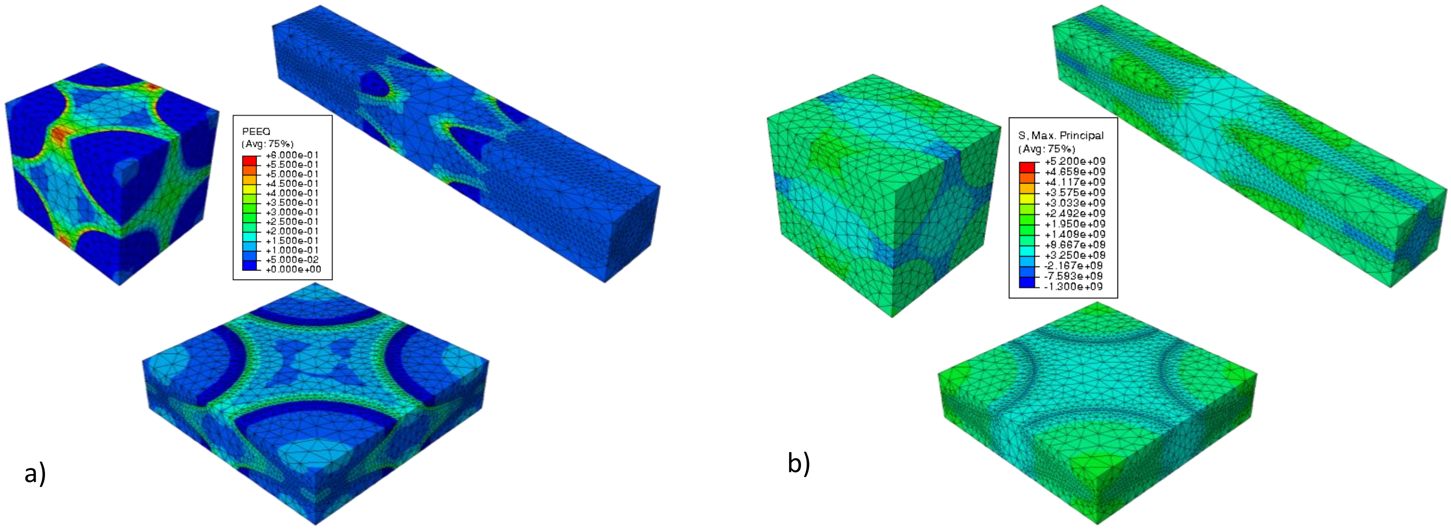

Figure 10. Contour plots for unit cells at a global strain of 0.1 with $V_{\alpha'}$ of 30%, θ of 0° of a) accumulated plastic strain and b) maximum principal stress

The variation of p at the particle pole located on the revolution axis (see Figure 11.a) is shown in Figures 11.b and 11.c as a function of the macroscopic applied strain. Figure 11.b is for $\theta = 0°$ and Figure 11.c is for $\theta = 90°$. For the 0° or 90° orientations, p is the highest for a prolate particle and the lowest for an oblate particle, as a result of the difference of particle curvature: the curvature is the highest for a prolate particle with sharp particle tip compared to the smoother curvature of an oblate particle pole.

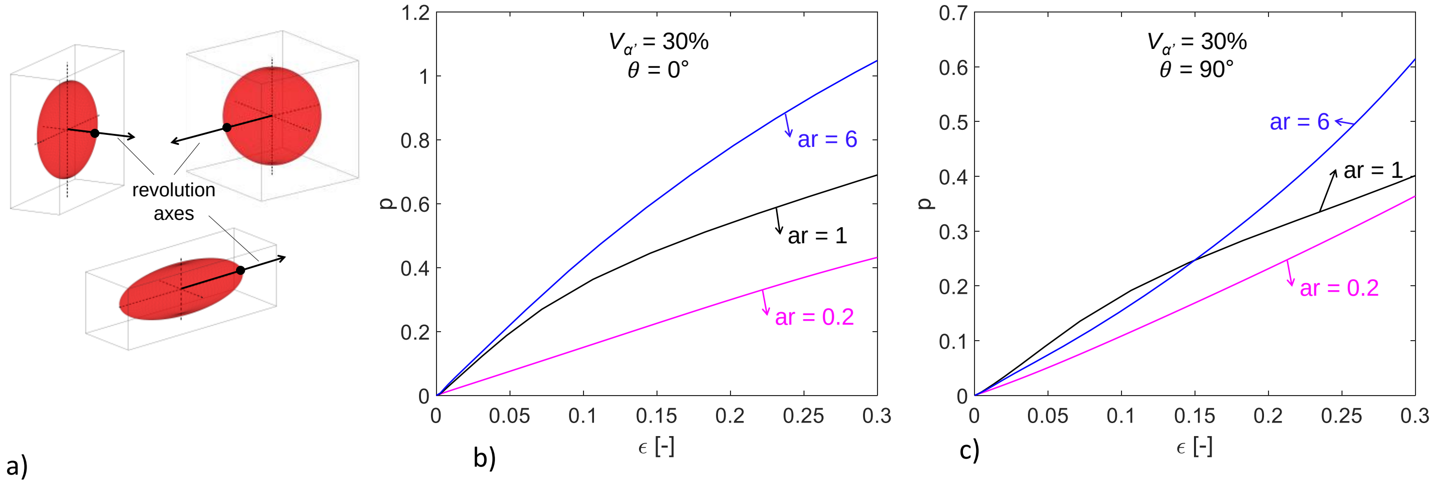

Figure 11. Local equivalent strain at the pole of the particle located on the revolution axis as shown in a) as a function of globa strain for different aspect ratios ($V_{\alpha'}$ = 30%) for: b) θ = 0°, c) θ = 90°

The variation of the stress triaxiality, maximum principal stress and damage indicator D are represented as a function of the macroscopic strain ε for different aspect ratios in Figure 12. The results are given at the pole following the logic of Figure 11. The stress triaxiality is positive for 0° since the pole region is in tension and it is negative for 90° due to compression. The maximum principal stress follows the same trend, apart from a first increase at 90° at very small strains within the elastic regime. Even if p is relatively similar for both angles, the pole is a critical damage spot at 0° where D reaches high values.

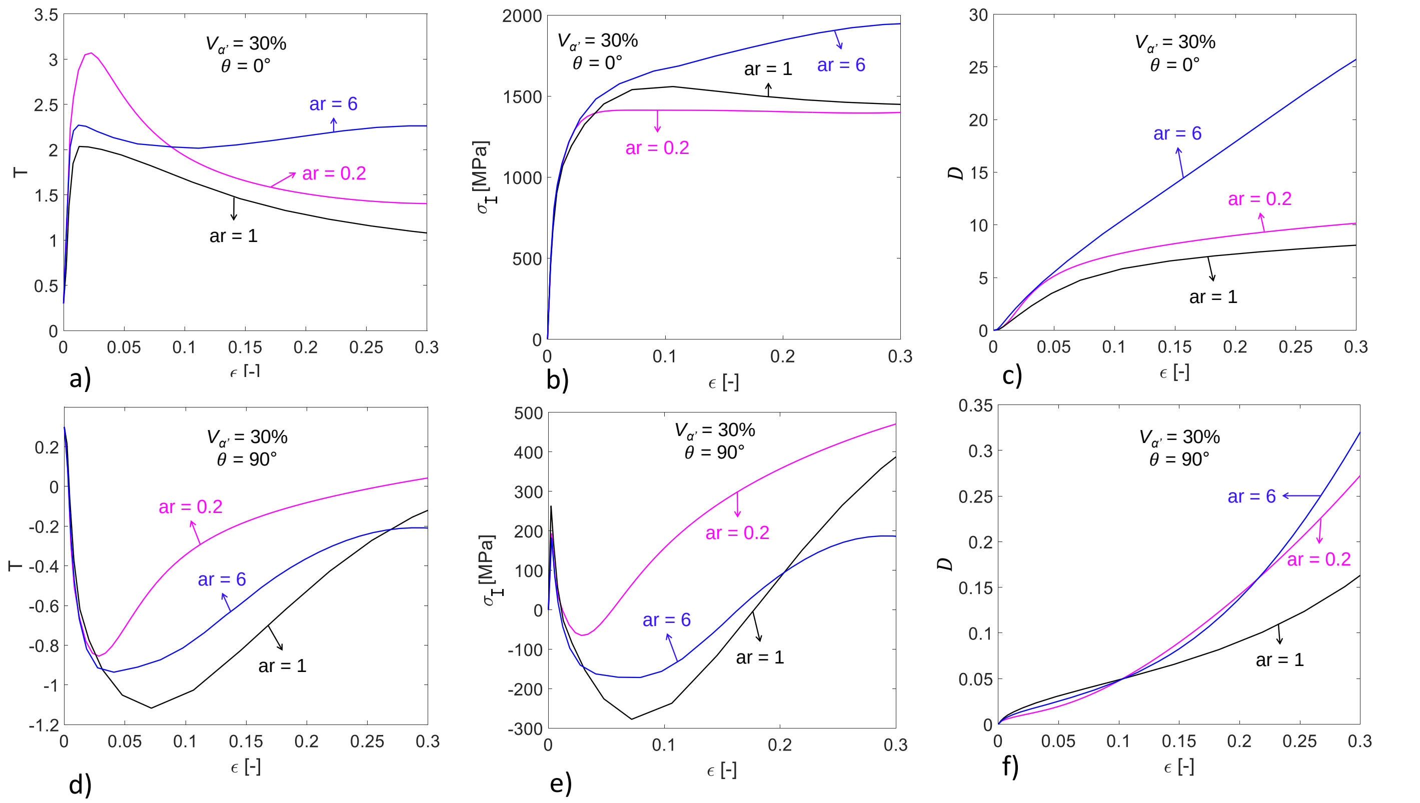

Figure 12. Evolution with strain of a) the stress triaxiality for θ = 0°, b) the maximum principal stress for θ = 0°, c) the damage indicator D for θ = 0°, d) the stress triaxiality for θ = 90°, e) the maximum principal stress for θ = 90°, f) the damage indicator D for θ = 90°

4. DISCUSSION

An important conclusion from Section 3 is that second phase morphology plays a minor role on the overall elastoplastic material behavior in the case of a uniform distribution of orientations. Contrarily, experimental trends indicate a positive effect of an elongated second phase morphology on strength and ductility, e.g. in (Das and Chattopadhyay, 2009) or (Pierman et al., 2014). The main reason for which the present model does not capture this trend is probably related to the absence of any internal length in the analysis. By changing morphology from an equiaxed to a platelet-like microstructure, the absolute spacing between particles decreases (refinement effect), which may impact the plastic flow behavior through a larger contribution of geometrically necessary dislocations accumulating near interfaces. The impact of microstructure refinement on the behavior of dual-phase steels has been addressed for instance by Delincé et al. (2007) showing the possibility to attain an optimum strength-ductility balance when playing with both martensitic volume fraction and ferrite grain size. The refinement effect can also directly impact the magnitude of the residual stresses generated during processing (Kadkhodapour et al., 2011a; Ramazani et al., 2013), which were neglected in this study as well. Now, the present results show that dual-phase microstructures with preferential alignment of elongated second phase particles can lead to significant effects on the hardening behavior. This could potentially be useful in applications where the main loading direction is fixed and in which one could beneficially use some controlled particle morphology anisotropy.

Other interesting conclusions can be drawn from the results shown in Section 3, regarding the local fields and their impact on damage and fracture toughness. The results of Figures 11 and 12 suggest that void nucleation by interface decohesion (mainly dictated by the amplitude of the maximum interface normal stress and accumulated plastic strain), and void growth (mainly dictated by stress triaxiality and accumulated plastic strain) are both expected to preferentially proceed at the particle pole located along the direction of loading (for θ = 0° or θ = 90°). Indeed, the ferrite regions near the interface typically exhibit the largest strains due to the abrupt change in properties (see Figure 10). This explains why damage often initiates by interface decohesion in dual-phase steels as shown in

Figure 13 and in many literature papers (e.g. Landron et al., 2010; Kadkhodapour et al., 2011c), and in particular at the poles of the elongated particles.

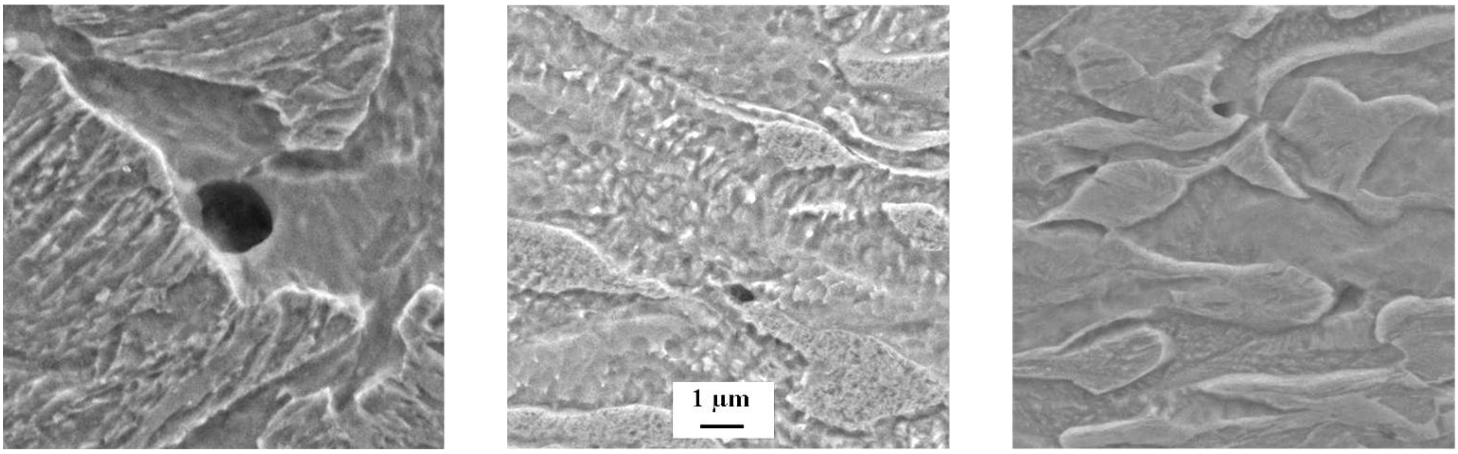

Figure 13. Void nucleation by decohesion in dual-phase steels (taken from Pierman (2013))

Moreover, and this is at the core of the objective of the present study, Figures 11 and 12 show that large differences in local quantities occur at a given pole depending on the aspect ratio and orientation of the particles. A first reason is that stress and strain states at a given location in the matrix near the interface depend on the curvature of the particle (see Section 3.3.). Second, the relative confinement of the plasticity in the matrix at the particle tip also changes with the aspect ratio. Third, the solicitation at a given point changes with orientation. For instance, under loading at 0°, the ferrite at the pole along the revolution axis undergoes large tensile stresses compensating for the small martensite deformation; under loading at 90°, it will be compressed against the martensite, which resists contraction in the direction perpendicular to the tensile loading. For this pole, 0° will lead to early decohesion due to a high interface normal stress and large accumulated plastic strain and accelerated void growth due to a high stress triaxiality and accumulated plastic strain. At 90°, damage will not develop at the pole, protected by a negative maximum principal stress and a negative stress triaxiality.

The previous considerations suggest that, in an aggregate of grains with elongated/flat particles of different orientations, the variation of local fields from grain to grain will lead to a very heterogeneous damage behavior at this scale, with early nucleation of voids and accelerated void growth in some grains compared to others, in turn leading to early onset of void coalescence in the highly damaged grains. However, fracture will need a second level of coalescence in between the highly damaged grains. This suggests that two length scales are at play during the fracture process: one associated to particle spacing (as discussed above) and one associated to the primary austenite grain size. The need for large-scale void coalescence between grains at the second length scale could lead to large fracture strains as demonstrated by (Pierman, 2013) for dual-phase steels with platelet-like microstructure. Regarding fracture toughness, the critical J-integral at cracking scales with the internal length scale dominating the failure process, e.g. in (Pardoen and Hutchinson, 2003) or (Pineau et al., 2016). A similar two-stage process was for instance recently addressed by Hannard et al. (2018) on Al alloys and could also be the reason for the high fracture toughness as also found experimentally by (Pierman, 2013). In metallurgical practice, increasing the time and/or temperature of the first step of the heat treatment for a platelet-like microstructure would lead to a larger primary austenite grain size and, potentially, if the reasoning above is valid, to a higher resistance to cracking as quantified both by the fracture strain and fracture toughness.

At last, in addition to the aforementioned absence of internal length, a few other limitations of the model should however be kept in mind as there are no direct experimental comparisons that can be made at this stage. Some limitations are intrinsic to the model. For instance, the grains are all assumed to be subject to macroscopically uniaxial tension, driven by the same macroscopic strain. In other words, we made an iso-strain assumption in direction 1, and an iso-stress (zero-stress) assumption regarding all the other components of stress (in the macroscopic coordinate system). This assumption was needed to solve each unit cell problem independently, and thereby to reduce the computational cost. An alternative strategy could be to consider a true iso-strain assumption, in which case the iterations on the a priori unknown values of the macroscopic strain components should be carried out after averaging the stress response over all unit cells. This would thus require the simultaneous numerical solution of all the unit cells problems, which would dramatically increase the computational cost of the simulation. However, it is not clear whether a true iso-strain simulation would be more realistic than the adopted strategy. A probably more accurate approach would be to adopt a self-consistent scheme to partition the macroscopic strain among the unit cells. In a self-consistent scheme, the average strain of each unit cell would be determined by treating it as an isolated inclusion in an infinite medium having the a-priori unknown properties of the whole aggregate. Such an approach would also bring about a large computational cost. Moreover, since periodic conditions are used in each unit cell, the local fields at interfaces between zones with particles oriented differently are not accounted for. The model also does not capture long range effects such as shear band development at meso or macro-scale.

Furthermore, some aspects are not taken into account in this study, although they can be addressed in the framework of the model. For instance, the previously mentioned initial accumulation of dislocations at interfaces due to austenite-to-martensite transformation and the associated residual stress and gradient of hardness were not taken into account in this analysis. The presence of residual stress resulting from processing can be simulated by subjecting the unit cells to inhomogeneous thermal dilation mimicking the transformation strain. The effect of chemical inhomogeneities on the mechanical properties could also be easily incorporated by using spatially dependent hardening properties. The effect of martensite connectivity could be investigated at any low to moderate volume fraction, for example by considering percolating star-like network (e.g. Bugat et al., 1999) of martensite within the unit cell. For instance, Landron et al. (2012) observed islands of interconnected martensite in a steel with a martensite volume fraction equal to 11% using holotomography. In order to account for the refinement effect, a strain gradient plasticity model could be adopted, see e.g. (Mazzoni-Leduc et al., 2008; Pardoen and Massart, 2012). Finally, one could consider using crystal plasticity theory to describe the ferrite and martensite constitutive behavior, instead of J2 plasticity theory. Choi et al. (2013) and Pagenkopf et al. (2016) have compared FE calculations with an isotropic model and a crystal plasticity model, respectively, and found that the computed local stress fields were significantly different. Varying the crystallographic orientations from grain to grain would introduce even more heterogeneities, with probable impact on the damage behavior. However, there is no reason to expect that the use of more refined constitutive models would change the conclusion that particle shape has a limited impact on the elastoplastic behavior in the case of uniform orientation distribution and absence of change of the internal microstructural length.

5. CONCLUSIONS AND PERSPECTIVES

Early works addressing the modeling of the link between microstructure and mechanical properties of dual-phase steels focused mainly on martensite volume fraction and on carbon content and rarely on particle morphology. The aim of this work was to shed light on the impact of particle morphology and orientation on the plastic behavior and damage of dual-phase steels in order to ultimately help in the prediction of mechanical properties and guide the processing of improved steels. The conclusions may nevertheless be applied to other metals comprising two phases of different hardness.

The modeling strategy is based on a two-level unit cell computational approach, which constitutes an efficient tool to study local and effective behavior while avoiding computationally intensive full FE simulations on multiparticle RVEs. The main findings are the following:

- Regardless of the value of the particle aspect ratio, unit cells loaded at a 45° angle relative to the revolution axis exhibit the highest uniform elongation and lowest tensile strength. Loading along 0° or a 90° orientation leads to the opposite trend.
- The effect of the loading angle on the mechanical properties (i.e. the anisotropy) increases as the aspect ratio of the particle differs from 1. In the case of a ferritic matrix (martensite volume fractions lower than 50%), the tensile strength increases and the uniform elongation decreases as the aspect ratio departs from 1. In the case of a martensitic matrix (martensite volume fractions larger than 50%), the opposite trend is observed.
- Even though the impact of particle aspect ratio is significant at a given loading angle, the particle shape has relatively limited impact on the effective behavior of an aggregate of grains with a random distribution of particle orientations. The effects found experimentally are presumably related to a microstructure refinement effect.

These results suggest that producing microstructures with preferential orientation of the second phase (for example by cold rolling) could be used to act on both ductility and strength. Despite having a small effect on plastic behavior of the aggregate, the morphology, orientation and martensite volume fraction largely influence the local mechanical fields and, thereby, lead to important stress and strain inhomogeneities, which control the damage process. We anticipate that damage in dual-phase steels with Thomas fiber microstructures develop in a two-stage process, first in some grains with specific orientation leading to fast local coalescence events, followed by larger-scale coalescence between damaged grains. This two-stage process might be the reason for the good cracking resistance of dual-phase steels with a platelet-like microstructure.

ACKNOWLEDGMENTS

This work was supported by the Interuniversity Attraction Poles Program from the Belgian State through the Belgian Policy agency, contract IAP7/21 "INTEMATE", ArcelorMittal and the UCL. Computational resources have been provided by the supercomputing facilities of the Université catholique de Louvain (CISM/UCL) and the Consortium des Équipements de Calcul Intensif en Fédération Wallonie Bruxelles (CÉCI) funded by the Fond de la Recherche Scientifique de Belgique (F.R.S.-FNRS) under convention 2.5020.11.

REFERENCES

- ABAQUS 6.12/Standard User's Manual. Pawtucket (RI): Hibbit, Karlsson and Sorensen Inc.; 2012.
- Abid, N.H., Abu Al-Rub, R.K., Palazotto, A.N., 2017. Micromechanical finite element analysis of the effects of martensite morphology on the overall mechanical behavior of dual phase steel. International Journal of Solids and Structures 104-105, 8-24. https://doi.org/10.1016/j.ijsolstr.2016.11.005
- Abid, N.H., Abu Al-Rub, R.K., Palazotto, A.N., 2015. Computational modeling of the effect of equiaxed heterogeneous microstructures on strength and ductility of dual phase steels. Computational Materials Science 103, 20-37. https://doi.org/10.1016/j.commatsci.2015.02.051
- Amirmaleki, M., Samei, J., Green, D.E., van Riemsdijk, I., Stewart, L., 2016. 3D micromechanical modeling of dual phase steels using the representative volume element method. Mechanics of Materials 101, 27-39. https://doi.org/10.1016/j.mechmat.2016.07.011
- Bag, A., Ray, K.K., Dwarakadasa, E.S., 1999. Influence of martensite content and morphology on tensile and impact properties of high-martensite dual-phase steels. Metallurgical and Materials Transactions A 30, 1193-1202. https://doi.org/10.1007/s11661-999-0269-4
- Bai, Y., Wierzbicki, T., 2008. A new model of metal plasticity and fracture with pressure and Lode dependence. International Journal of Plasticity 24, 1071-1096. https://doi.org/10.1016/j.ijplas.2007.09.004

- Bong, H.J., Lim, H., Lee, M.-G., Fullwood, D.T., Homer, E.R., Wagoner, R.H., 2017. An RVE procedure for micromechanical prediction of mechanical behavior of dual-phase steel. Materials Science and Engineering: A 695, 101-111. https://doi.org/10.1016/j.msea.2017.04.032
- Bouaziz, O., Zurob, H., Huang, M., 2013. Driving force and logic of development of advanced high strength steels for automotive applications. steel research international 84, 937-947. https://doi.org/10.1002/srin.201200288
- Bugat, S., Besson, J., Pineau, A., 1999. Micromechanical modeling of the behavior of duplex stainless steels. Computational Materials Science 16, 158-166. https://doi.org/10.1016/S0927-0256(99)00058-0
- Calcagnotto, M., Ponge, D., Raabe, D., 2010. Effect of grain refinement to 1 µm on strength and toughness of dual-phase steels. Materials Science and Engineering: A 527, 7832-7840. https://doi.org/10.1016/j.msea.2010.08.062
- Chang, P.-H., Preban, A.G., 1985. The effect of ferrite grain size and martensite volume fraction on the tensile properties of dual phase steel. Acta Metallurgica 33, 897-903. https://doi.org/10.1016/0001-6160(85)90114-2
- Choi, K.S., Liu, W.N., Sun, X., Khaleel, M.A., 2009. Influence of martensite mechanical properties on failure mode and ductility of dual-phase steels. Metallurgical and Materials Transactions A 40, 796-809. https://doi.org/10.1007/s11661-009-9792-6
- Choi, S.-H., Kim, E.-Y., Woo, W., Han, S.H., Kwak, J.H., 2013. The effect of crystallographic orientation on the micromechanical deformation and failure behaviors of DP980 steel during uniaxial tension. International Journal of Plasticity 45, 85-102. https://doi.org/10.1016/j.ijplas.2012.11.013
- Das, D., Chattopadhyay, P.P., 2009. Influence of martensite morphology on the work-hardening behavior of high strength ferrite-martensite dual-phase steel. Journal of Materials Science 44, 2957-2965. https://doi.org/10.1007/s10853-009-3392-0
- Davies, R.G., 1978. Influence of martensite composition and content on the properties of dual phase steels. Metallurgical Transactions A 9, 671-679. https://doi.org/10.1007/BF02659924
- de Geus, T.W.J., Peerlings, R.H.J., Geers, M.G.D., 2015. Microstructural topology effects on the onset of ductile failure in multi-phase materials – a systematic computational approach. International Journal of Solids and Structures 67-68, 326-339. https://doi.org/10.1016/j.ijsolstr.2015.04.035

- Delannay, L., Jacques, P.J., Kalidindi, S.R., 2006. Finite element modeling of crystal plasticity with grains shaped as truncated octahedrons. International Journal of Plasticity 22, 1879-1898. https://doi.org/10.1016/j.ijplas.2006.01.008
- Delincé, M., Bréchet, Y., Embury, J.D., Geers, M.G.D., Jacques, P.J., Pardoen, T., 2007. Structure-property optimization of ultrafine-grained dual-phase steels using a microstructure-based strain hardening model. Acta Materialia 55, 2337-2350. https://doi.org/10.1016/j.actamat.2006.11.029
- Deng, D., 2009. FEM prediction of welding residual stress and distorsion in carbon steel considering phase transformation effects. Materials & Design 30, 359-366. https://doi.org/10.1016/j.matdes.2008.04.052
- Erice, B., Gálvez, F., 2014. A coupled elastoplastic-damage constitutive model with Lode angle dependent failure criterion. International Journal of Solids and Structures 51, 93-110. https://doi.org/10.1016/j.ijsolstr.2013.09.015
- Hannard, F., Simar, A., Maire, E., Pardoen, T., 2018. Quantitative assessment of the impact of second phase particle arrangement on damage and fracture anisotropy. Acta Materialia 148, 456-466. https://doi.org/10.1016/j.actamat.2018.02.003
- Hatami, M.K., Pardoen, T., Lacroix, G., Berke, P., Jacques, P.J., Massart, T.J., 2017. Towards ultra-high ductility TRIP-assisted multiphase steels controlled by strain gradient plasticity effects. Journal of the Mechanics and Physics of Solids 98, 201-221. https://doi.org/10.1016/j.jmps.2016.09.006
- Huang, T.T., Gou, R.B., Dan, W.J., Zhang, W.G., 2016. Strain-hardening behaviors of dual phase steels with microstructure features. Materials Science and Engineering: A 672, 88-97. https://doi.org/10.1016/j.msea.2016.06.066
- Kadkhodapour, J., Schmauder, S., Raabe, D., Ziaei-Rad, S., Weber, U., Calcagnotto, M., 2011a. Experimental and numerical study on geometrically necessary dislocations and non-homogeneous mechanical properties of the ferrite phase in dual phase steels. Acta Materialia 59, 4387-4394. https://doi.org/10.1016/j.actamat.2011.03.062
- Kadkhodapour, J., Butz, A., Ziaei-Rad, S., Schmauder, S., 2011b. A micro mechanical study on failure initiation of dual phase steels under tension using single crystal plasticity model. International Journal of Plasticity 27, 1103-1125. https://doi.org/10.1016/j.ijplas.2010.12.001

- Kadkhodapour, J., Butz, A., Ziaei Rad, S., 2011c. Mechanisms of void formation during tensile testing in a commercial, dual-phase steel. Acta Materialia 59, 2575-2588. https://doi.org/10.1016/j.actamat.2010.12.039
- Kim, N.J., Thomas, G., 1981. Effects of morphology on the mechanical behavior of a dual phase Fe/2Si/0.1C steel. Metallurgical Transactions A 12, 483-489. https://doi.org/10.1007/BF02648546
- Lai, Q., Bouaziz, O., Gouné, M., Brassart, L., Verdier, M., Parry, G., Perlade, A., Bréchet, Y., Pardoen, T., 2015. Damage and fracture of dual-phase steels : Influence of martensite volume fraction. Materials Science and Engineering: A 646, 322-331. https://doi.org/10.1016/j.msea.2015.08.073
- Lai, Q., Brassart, L., Bouaziz, O., Gouné, M., Verdier, M., Parry, G., Perlade, A., Bréchet, Y., Pardoen, T., 2016. Influence of martensite volume fraction and hardness on the plastic behavior of dual-phase steels: Experiments and micromechanical modeling. International Journal of Plasticity 80, 187-203. https://doi.org/10.1016/j.ijplas.2015.09.006
- Landron, C., Bouaziz, O., Maire, E., Adrien, J., 2010. Characterization and modeling of void nucleation by interface decohesion in dual phase steels. Scripta Materialia 63, 973-976. https://doi.org/10.1016/j.scriptamat.2010.07.021
- Landron, C., Maire, E., Adrien, J., Suhonen, H., Cloetens, P., Bouaziz, O., 2012. Non-destructive 3-D reconstruction of the martensitic phase in a dual-phase steel using synchrotron holotomography. Scripta Materialia 66, 1077-1080. https://doi.org/10.1016/j.scriptamat.2012.03.003
- Lingamanaik, S.N., Chen, B.K., 2011. Thermo-mechanical modelling of residual stresses induced by martensitic phase transformation and cooling during quenching of railway wheels. Journal of Processing Technology 211, 1547-1552. https://doi.org/10.1016/j.jmatprotec.2011.04.007
- Mahnken, R., Schneidt, A., Antretter, T., 2009. Macro modelling and homogenization for transformation induced plasticity of a low-alloy steel. International Journal of Plasticity 25, 183-204. https://doi.org/10.1016/j.ijplas.2008.03.005
- Marder, A.R., 1982. Deformation characteristics of dual-phase steels. Metallurgical Transactions A 13, 85-92. https://doi.org/10.1007/BF02642418

- Mazinani, M., Poole, W.J., 2007. Effect of martensite plasticity on the deformation behavior of a low-carbon dual-phase steel. Metallurgical and Materials Transactions A 38, 328-339. https://doi.org/10.1007/s11661-006-9023-3
- Mazzoni-Leduc, L., Pardoen, T., Massart, T.J., 2008. Strain gradient plasticity analysis of transformation induced plasticity in multiphase steels. International Journal of Solids and Structures 45, 5397-5418. https://doi.org/10.1016/j.ijsolstr.2008.05.025
- Moan, G.D., Embury, J.D., 1979. A study of the bauschinger effect in Al-Cu Alloys. Acta Metallurgica 27, 903-914. https://doi.org/10.1016/0001-6160(79)90125-1
- Ognedal, A.S., Clausen, A.H., Berstad, T., Seelig, T., Hopperstad, O.S., 2014. Void nucleation and growth in mineral-filled PVC – An experimental and numerical study. International Journal of Solids and Structures 51, 1494-1506. https://doi.org/10.1016/j.ijsolstr.2013.12.042
- Pagenkopf, J., Butz, A., Wenk, M., Helm, D., 2016. Virtual testing of dual-phase steels: Effect of martensite morphology on plastic flow behavior. Materials Science and Engineering: A 674, 672-686. https://doi.org/10.1016/j.msea.2016.07.118
- Pardoen, T., Hutchinson, J.W., 2003. Micromechanics-based model for rends in toughness of ductile metals. Acta Materialia 51, 133-148. https://doi.org/10.1016/S1359-6454(02)00386-5
- Pardoen, T., Massart, T.J., 2012. Interface controlled plastic flow modelled by strain gradient plasticity theory. Comptes Rendus Mécanique 340, 247-260. https://doi.org/10.1016/j.crme.2012.02.008
- Paul, S.K., Kumar, A., 2012. Micromechanics based modeling to predict flow behavior and plastic strain localization of dual phase steels. Computational Materials Science 63, 66-74. https://doi.org/10.1016/j.commatsci.2012.05.061
- Pierman, A.-P., Bouaziz, O., Pardoen, T., Jacques, P.J., Brassart, L., 2014. The influence of microstructure and composition on the plastic behaviour of dual-phase steels. Acta Materialia 73, 298-311. https://doi.org/10.1016/j.actamat.2014.04.015
- Pierman, A.-P., 2013. Micromechanical study of the influence of the microstructure and composition on the plastic flow and damage properties of Dual-Phase steels. Université catholique de Louvain.
- Pineau, A., Benzerga, A.A., Pardoen, T., 2016. Failure of metals I: Brittle and ductile fracture. Acta Materialia 107, 424-483. https://doi.org/10.1016/j.actamat.2015.12.034

- Ramazani, A., Mukherjee, K., Schwedt, A., Goravanchi, P., Prahl, U., Bleck, W., 2013. Quantification of the effect of transformation-induced geometrically necessary dislocations on the flow-curve modelling of dual-phase steels. International Journal of Plasticity 43, 128-152. https://doi.org/10.1016/j.ijplas.2012.11.003
- Ramazani, A., Mukherjee, K., Prahl, U., Bleck, W., 2012. Modelling the effect of microstructural banding on the flow curve behavior of dual-phase (DP) steels. Computational Materials Science 52, 46-54. https://doi.org/10.1016/j.commatsci.2011.05.041
- Ramos, L.F., Matlock, D.K., Krauss, G., 1979. On the deformation behavior of dual-phase steels. Metallurgical Transactions A 10, 259-261. https://doi.org/10.1007/BF02817636
- Rice, J.R., Tracey, D.M., 1969. On the ductile enlargement of voids in triaxial stress fields. Journal of the Mechanics and Physics of Solids 17, 201-217. https://doi.org/10.1016/0022-5096(69)90033-7
- Sakaki, T., Sugimoto, K., Fukuzato, T., 1983. Role of internal stress for continuous yielding of dual-phase steels. Acta Metallurgica 31, 1737-1746. https://doi.org/10.1016/0001-6160(83)90172-4
- Sarosiek, A.M., Owen, W.S., 1984. The work hardening of dual-phase steels at small plastic strains. Materials Science and Engineering 66, 13-34. https://doi.org/10.1016/0025-5416(84)90138-1
- Sarwar, M., Priestner, R., 1996. Influence of ferrite-martensite microstructural morphology on tensile properties of dual-phase steel. Journal of Materials Science 31, 2091-2095. https://doi.org/10.1007/BF00356631
- Schöberl, J., 1997. NETGEN An advancing front 2D/3D-mesh generator based on abstract rules. Computing and Visualization in Science 1, 41-52. https://doi.org/10.1007/s007910050004
- Speich, G.R., Miller, R.L., 1979. Mechanical properties of ferrite-martensite steels. In Structure and Properties of Dual Phase Steels, The Metallurgical Society of AIME, 145-182.
- Sun, S., Pugh, M., 2002. Properties of thermomechanically processed dual-phase steels containing fibrous martensite. Materials Science and Engineering: A 335, 298-308. https://doi.org/10.1016/S0921-5093(01)01942-6
- Sun, X., Choi, K.S., Liu, W.N., Khaleel, M.A., 2009. Predicting failure modes and ductility of dual phase steels using plastic strain localization. International Journal of Plasticity 25, 1888-1909. https://doi.org/10.1016/j.ijplas.2008.12.012

- Tasan, C.C., Diehl, M., Yan, D., Bechtold, M., Roters, F., Schemmann, L., Zheng, C., Peranio, N., Ponge, D., Koyama, M., Tsuzaki, K., Raabe, D., 2015. An overview of dual-phase steels: Advances in microstructure-oriented processing and micromechanically guided design. Annual Review of Materials Research 45, 391-431. https://doi.org/10.1146/annurev-matsci-070214-021103
- Tasan, C.C., Hoefnagels, J.P.M., Diehl, M., Yan, D., Roters, F., Raabe, D., 2014. Strain localization and damage in dual phase steels investigated by coupled *in-situ* deformation experiments and crystal plasticity simulations. International Journal of Plasticity 63, 198-210. https://doi.org/10.1016/j.ijplas.2014.06.004
- Tomita, Y., 1990. Effect of morphology of second-phase martensite on tensile properties of Fe-0.1C dual phase steels. Journal of Materials Science 25, 5179-5184. https://doi.org/10.1007/BF00580148
- Xue, L., 2007. Damage accumulation and fracture initiation in uncracked ductile solids subject to triaxial loading. International Journal of Solids and Structures 44, 5163-5181. https://doi.org/10.1016/j.ijsolstr.2006.12.026
- Zarei, S., Nedoushan, R.J., Atapour, M., 2016. The sources of the micro stress and strain inhomogeneity in dual phase steels. Materials Science and Engineering: A 674, 384-396. https://doi.org/10.1016/j.msea.2016.07.028
- Zhang, F., Ruimi, A., Wo, P.C., Field, D.P., 2016. Morphology and distribution of martensite in dual phase (DP980) steel and its relation to the multiscale mechanical behavior. Materials Science and Engineering: A 659, 93-103. https://doi.org/10.1016/j.msea.2016.02.048